scientific reports

Check for updates

OPEN

In-vitro and in-vivo assessment of biocompatibility and efficacy of ostrich eggshell membrane combined with platelet-rich plasma in Achilles tendon regeneration

Omid Koohi-Hosseinabadi[1,2], Reza Shahriarirad[3,4]✉, Amireza Dehghanian[5], Laleh Amini[6], Sajjad Barzegar[7], Afrooz Daneshparvar[8], Omid Alavi[9], Seyedeh-Parvin Khazraei[10], Saba Hosseini[11], Ali Arabi Monfared[12], Roya Khorram[13], Nader Tanideh[14,15]✉ & Soheil Ashkani-Esfahani[16,17,18]

Tendon injuries present significant medical, social, and economic challenges globally. Despite advancements in tendon injury repair techniques, outcomes remain suboptimal due to inferior tissue quality and functionality. Tissue engineering offers a promising avenue for tendon regeneration, with biocompatible scaffolds playing a crucial role. Ostrich eggshell membrane (ESM), characterized by a strong preferential orientation of calcite crystals, forms a semipermeable polymer network with excellent mechanical properties compared to membranes from other bird species, emerging as a potential natural scaffold candidate. Coupled with platelet-rich plasma (PRP), known for its regenerative properties, ESM holds promise for improving tendon repair. This study aims to evaluate the biocompatibility and efficacy of an ESM-PRP scaffold in treating Achilles tendon ruptures, employing in vitro and in vivo assessments to gauge its potential in tendon regeneration in living organisms. Ostrich ESM was prepared from pathogen-free ostrich eggs, sterilized with UV radiation and prepared in desired dimensions before implantation (1.5 × 1 cm). High-resolution scanning electron microscopy (HRSEM) was utilized to visualize the sample morphology and fiber bonding. In vitro biocompatibility was assessed using the MTT assay and DAPI staining, while in vivo biocompatibility was evaluated in a rat model. For the in vivo Achilles tendinopathy assay, rats were divided into groups and subjected to AT rupture followed by treatment with ESM, PRP, or a combination. SEM was employed to evaluate tendon morphology, and real-time PCR was conducted to analyze gene expression levels. The in vivo assay indicated that the ESM scaffold was safe for an extended period of 8 weeks, showing no signs of inflammation based on histopathological analysis. In the Achilles tendon rupture model, combining ESM with PRP enhanced tendon healing after 14 weeks post-surgery. This finding was supported by histopathological, morphological, and mechanical evaluations of tendon tissues compared to normal tendons, untreated tendinopathy, and injured tendons treated with the ESM scaffold. Gene expression analysis revealed significantly increased expression of Col1a1, Col3a1, bFGF, Scleraxis (Scx), and tenomodulin in the ESM-PRP groups. The findings of our study demonstrate that the combination of Ostrich ESM with PRP significantly enhances AT repair and is a biocompatible scaffold for the application in living organisms.

Keywords Achilles tendon ruptures, Biocompatibility, Ostrich eggshell membrane, Platelet-rich plasma, Tendon injuries, Tissue engineering

[1]Laparoscopy Research Center, Shiraz University of Medical Sciences, Shiraz, Iran. [2]Central Research Laboratory, Shiraz University of Medical Sciences, Shiraz, Iran. [3]Thoracic and Vascular Surgery Research Center, Shiraz University of Medical Sciences, Shiraz, Iran. [4]School of Medicine, Shiraz University of Medical Sciences, Shiraz, Iran. [5]Department of Pathology, School of Medicine, Shiraz University, Shiraz, Iran. [6]Department of Pathology, School of Veterinary Medicine, Shiraz University, Shiraz, Iran. [7]Department of Chemical Engineering, School of Chemical and Petroleum Engineering, Shiraz University, Shiraz, Iran. [8]Molecular Dermatology Research Center,

Shiraz University of Medical Sciences, Shiraz, Iran. [9]Department of Tissue Engineering and Applied Cell Sciences, School of Advanced Medical Sciences and Technologies, Shiraz University of Medical Sciences, Shiraz, Iran. [10]Cardiology Department, Shiraz University of Medical Sciences, Shiraz, Iran. [11]Department of Biology, Yazd University, Yazd, Iran. [12]Department of Medical Mycology, Faculty of Medical Sciences, Tarbiat Modares University, Tehran, Iran. [13]Bone and Joint Diseases Research Center, Department of Orthopedic Surgery, Shiraz University of Medical Sciences, Shiraz, Iran. [14]Stem Cells Technology Research Center, Shiraz University of Medical Sciences, P. O. Box: 7134845794, Shiraz, Iran. [15]Pharmacology Department, Shiraz Medical School, Shiraz University of Medical Sciences, Shiraz, Iran. [16]Foot and Ankle Research and Innovation Lab (FARIL), Department of Orthopaedic Surgery, Massachusetts General Hospital, Harvard Medical School, Boston, MA, USA. [17]Foot and Ankle Division, Department of Orthopaedic Surgery, Massachusetts General Hospital, Harvard Medical School, Boston, MA, USA. [18] Department of Orthopaedic Surgery, Massachusetts General Hospital, Harvard Medical School, Boston, MA, USA. ✉email: R.shahriari1995@gmail.com; tanidehn@sums.ac.ir; tanidehn@gmail.com

Tendon, a structurally complex tissue, serves the essential role of translating muscular contractions into joint movement by transmitting forces from muscle to bone[1]. Each year, approximately 60 thousand patients in the United States experience tendon injuries, posing significant medical, social, and economic challenges globally[2]. The Achilles tendon (AT) stands as the body's thickest and strongest tendon, forming from the merging of the gastrocnemius and soleus muscles[3,4]. Injuries to the AT are common among individuals engaging in vigorous physical activities like running and jumping, prevalent in sports such as volleyball, tennis, soccer, and badminton[5–10]. Sports-related Achilles tendinopathy often manifests as a complete rupture of the tendon[11], characterized by hypoxic and mucoid degeneration, tissue necrosis, limited vascular supply, cell necrosis, calcification, and irregular collagen fibers[12–14].

Despite advancements in tendon injury repair techniques, clinical outcomes remain suboptimal due to the inferior quality and functionality of the repaired tissue[15,16]. The process of tendon regeneration, such as following rotator cuff tears, is recognized as intricate and gradual, presenting a clinical challenge in achieving effective tendon repair. Factors such as patient age, tendon condition, and tear size contribute to varying re-rupture rates[17,18]. Throughout the healing process, excessive disorganized collagen deposition occurs, leading to the formation of scar tissue and adhesions between newly formed and adjacent tissues[19]. Moreover, there is an increase in collagen type III at the injury site during the healing phase[20]. These factors collectively diminish the mechanical properties of the repaired tendon, thereby elevating the risk of re-rupture later in life. The treatment of ruptured tendons has transitioned from nonsurgical techniques to open surgeries and now to minimally invasive methods. Despite lower re-rupture rates associated with surgical treatment, this approach still presents complications such as scar formation, infection risk, and prolonged recovery[21–23]. Currently, allograft and autograft reconstruction techniques are utilized for treating AT ruptures. However, allograft procedures may lead to rejection or disease transmission, while autografts are constrained by limited availability[24]. Consequently, there is an urgent and unmet need to address how to effectively and biologically repair injured tendons, including Achilles tendinopathy.

Tissue engineering and regenerative medicine, which involve the use of biocompatible scaffolds, offer new options for reconstructing damaged tendon tissues[25–27]. A wide range of natural and synthetic polymeric scaffolds have been utilized in regenerative medicine. However, these biomedical applications and tissue engineering regeneration strategies often lack cellular recognition[28,29]. A suitable scaffold must possess several essential properties, including biocompatibility, biodegradability, high mechanical strength, and non-toxicity[30–34]. Previous studies have explored the use of the amniotic membrane as a potential scaffold in tissue engineering; however, its limitations necessitate the search for a more suitable and cost-effective alternative[35].

Natural eggshell membrane (ESM) has emerged as a promising and valuable bioresource in tissue regeneration, attributed to its availability, biocompatibility, and low toxicity[36]. Proteins constitute the primary components of the inner ESM fibers, accounting for 80–85% of its composition. Each fiber comprises a core rich in collagen (types I, V, and X) and a cortex abundant in glycoproteins[37–44]. Additionally, previous studies have identified the presence of other proteins such as lysozyme[45], ovotransferrin[46], ovalbumin[47], ovocalyxin-36[48,49], desmozine[42], isodesmozine[50], osteopontin, sialoprotein, and keratin[51] within the ESM structure. Amino acids also contribute to the chemical composition of ESM, with proline, glutamic acid, glycine, serine, hydroxyproline, aspartic acid, valine, threonine, arginine, leucine, alanine, histidine, and lysine being among the amino acids found in ESM[52]. These components have been proven to assist in the healing of wound and tendons in previous studies[53–56]. Studies have also demonstrated anti-microbial activities of these components, such as ovocalyxin-36, lysozyme, and ovotransferrin[48,57]. Ostrich eggshell membrane represents an abundant industrial and household waste characterized by a strong preferential orientation of calcite crystals. Its structure forms a semipermeable polymer network with excellent mechanical properties compared to membranes from other bird species[58].

One popular strategy to stimulate regeneration in poorly healing tissues like tendons is the use of platelet-rich plasma (PRP)[59]. PRP is derived from centrifuging whole blood, resulting in a concentration of platelets rich in various growth factors such as transforming growth factor-b1, insulin-like growth factors 1 and 2, vascular endothelial growth factor (VEGF), basic fibroblast growth factor, and hepatocyte growth factor (HGF)[60–62]. These growth factors play crucial roles in platelet adhesion and activation, fibrin formation, and the release of intracellular stores, predominantly a-granules (50–80 a-granules per platelet), dense granules (3–5 granules per platelet), and lysosomes[63]. Previous studies have indicated that PRP initially inhibits excessive inflammation and subsequently promotes proliferation and maturation, while also enhancing fibroblast production and collagen synthesis in the early stages of treatment[64–66]. Over the long term, PRP leads to increased collagen and glycosaminoglycans content, enhanced collagen organization, metabolic activity, improved load to failure, and elastic modulus[62]. While several studies have reported the benefits of PRP injection for the treatment of AT injuries, few have investigated its effects in combination with a scaffold.

This study introduces a novel, completely natural scaffold composed of Ostrich ESM and PRP, designed to address AT rupture. The innovative use of ESM leverages its unique biological properties, offering a promising alternative for developing advanced tendon repair materials. The biocompatibility of ESM was rigorously evaluated through in vitro assays (MTT and DAPI staining) and in vivo implantation, confirming its safety and non-toxicity. Furthermore, the study investigated the scaffold's therapeutic potential in an in vivo AT rupture model, where the combination of ESM and PRP demonstrated significant regenerative effects. Comprehensive evaluations, including histopathological analysis, Scanning Electron Microscopy (SEM), and mechanical property assessments, underscored the scaffold's capacity to support tendon healing. These findings highlight the potential of ESM as a groundbreaking approach in tendon tissue engineering.

Materials and methods

Ostrich ECM

Preparation

Pathogen-free ostrich eggs were obtained from a local market. The eggs were rinsed with sterile distilled water and disinfected with ethanol. After removal of the albumin and yolk from eggs, the eggshells were washed several times with normal saline and the ESM were carefully peeled off from eggshells with sterile forceps. The detached ESM was then placed in normal saline for 1 to 2 h before being kept in a falcon for 24 h at −70 °C. Following this, the ECM were subjected to freeze-drying for 48 h until completely dried. Samples of membranes were sterilized with UV radiation and prepared in desired dimensions before implantation (1.5 × 1 cm).

ESM characterization

High-resolution scanning electron microscopy (TESCAN-vega3, TESCAN Czech Republic) was employed to visualize the sample morphology and fiber bonding. ESM scaffolds (1 cm^2) were sputter-coated with gold for 120 s before observation to reduce the charging effect. Images with different magnifications were captured to provide a better view of the fibers' morphology. The HRSEM micrographs were taken using a voltage of 5 kV[67,68].

In vitro biocompatibility

MTT assay

The MTT (3-(4,5-dimethylthiazol-2-yl)-2,5-diphenyltetrazolium bromide) colorimetric assay was used to investigate cell viability six days after seeding. 5000 seeded cells were used for each assay. Cell-seeded scaffolds were rinsed with PBS, and MTT solution at 0.5 mg/ml was added to each well and incubated for 4 h. The yellow MTT dye was reduced by the mitochondrial reductase enzyme in living cells to purple Formosan after the incubation period; the Formosan was then dissolved with 400 µl of DMSO, and its absorbance was measured with a spectrophotometer at 590 nm. The cell survival assessment was conducted on days 3 and 6 following cell culture as per previous studies[69,70].

DAPI staining

ESM samples were placed in a 24-well plate and treated with cells for 72 h. The procedure involved adding 2 ml of 4% paraformaldehyde to each well to fix the scaffolds at room temperature for 30 min. The paraformaldehyde was then removed, and 2 ml of 0.01 mol/l Phosphate Buffered Saline (PBS) was added to each well for rinsing for 5 min. The PBS was discarded and the process repeated. Subsequently, 5 µg/ml DAPI (Sigma) was added to each well, and the plate was covered and incubated in the dark for 5 min at room temperature. After incubation, DAPI was removed, and 2 ml of 0.01 mol/l PBS was added to each well for rinsing. The plate was rinsed for 10 min, and this step was repeated until no more dye could be removed. Cell residue was observed in random fields of view using a Leica laser confocal microscope (Leica Microsystems GmbH) and a normal light microscope. The present evaluation verified whether there was cell residue inside the scaffold. Additionally, HRSEM micrographs were taken using a voltage of 5 kV for a better view of the cells.

After being cultured for a predetermined period, the specimens with attached cells were gently rinsed three times in PBS and then immersed in PBS containing 2.0% glutaraldehyde for 4 h to fix the cells. Following fixation, they were rinsed three times with PBS for 10 min each. Subsequently, they underwent dehydration through a graded series of ethanol solutions (30%, 50%, 70%, 90%, and 95%) for 10 min each, followed by immersion in 100% ethanol for an additional 30 min. Afterward, the samples were air-dried for at least 10 h. The dry cell-seeded scaffolds were then mounted on aluminum stubs, sputter-coated with gold–palladium, and examined under a scanning electron microscope.

In vivo biocompatibility assay

Animals

For in vivo assessment, a total of 18 adult male Wistar rats weighing 180 ± 5 g were used in this experiment. The animals were housed in a controlled environment with a 12-hour light/12-hour dark cycle at 21 ± 1 °C and a humidity of 55 ± 5%. Prior to the experiments, a seven-day acclimatization period was provided. The rats were granted ad libitum access to food and water throughout the study period. All experimental procedures were ethically approved by the Ethics Committee of Shiraz Medical University under permission number M1310.

In vivo model

To assess the in vivo biocompatibility of the scaffolds, the prepared specimens were subcutaneously implanted. Eighteen male rats were evenly distributed into three groups for the experiment, which were sacrificed after the first, fourth, and eight week of scaffold implantation. Anesthesia was induced via intramuscular injection of 90 mg/kg ketamine HCl and 8 mg/kg xylazine. Sterile surgical technique was applied throughout the experiment. Prior to implantation, all scaffolds were sterilized using gamma radiation. The implantation site

was shaved and sterilized with Betadine. A transverse incision of approximately 2 cm was made on the dorsal side of each rat using a sterile surgical blade, followed by dissection of the underlying connective tissue. The prepared ECM scaffolds were then implanted into the subcutaneous tissue, and the incision was closed using 5.0 sutures (Fig. 1). Each rat was housed under standard conditions for a duration of eight weeks post-surgery and monitored for any clinical signs or symptoms. At weeks 1, 4, and 8 post-implantation, the rats were euthanized, and the implanted samples along with surrounding tissues were harvested and fixed in neutral buffered formalin 10% for subsequent histological studies.

Histopathologic assay

For histological analysis, the skin region implanted with scaffolds and its surrounding tissues were immersed in a 10% formalin solution and fixed for 48 h prior to routine processing. Subsequently, they underwent processing and embedding in paraffin blocks. Thick layers (5 mm longitudinal sections) were prepared using a microtome and stained with hematoxylin and eosin (H&E). Microscopic images were then captured using an Olympus microscope (model BX53F, Japan). The specimens were evaluated by a blind pathologist for inflammation, cell infiltration, scar tissue formation, and neovascularization. The average of these values was determined for each animal, and a median score for each group and organ was assessed[71].

In vivo Achilles tendinopathy assay

Animal

Fifty adult male Wistar rats (180 ± 5 g body weight) were used for this experiment. Similar to our previous assessment, the animals were housed in a controlled environment with a 12-hour light/12-hour dark cycle at 21 ± 1 °C and a humidity of 55 ± 5%. Prior to the experiments, a seven-day acclimatization period was provided, during which the rats had ad libitum access to food and water.

In vivo model

The fifty rats were divided into five groups:

Control Positive (CP) Group: Normal control group where ten rats were kept without injuries.

Control Negative (CN) Group: Negative control group where AT rupture was induced, but no graft was applied. The AT was removed, and the sides of the rupture were sutured together.

Scaffold (SC) Group: Treatment group where double-layered ESM was grafted onto the ruptured tendon by suturing on both sides.

Scaffold PRP (SP) Group (SP): Treatment group where double-layered ESM with PRP was grafted onto the injured site by suturing on both sides.

Scaffold Self-derived PRP (SS) Group: Treatment group where double-layered ESM with self-derived PRP was grafted onto the ruptured AT by suturing on both sides.

To induce AT rupture, the rats were anesthetized with an intramuscular injection of ketamine (90 mg/kg) and xylazine (8 mg/kg). The area around the ankle was shaved and sterilized with Betadine. A small incision was made in the skin above the AT, and the tendon was sliced using a scalpel (1.5 cm). The incision was closed with 3.0 mm propylene suture, and each rat was housed under standard conditions for fourteen weeks post-surgery. The general condition of the rats was evaluated weekly post-surgery. After 14 weeks, the gait of the rats was evaluated, followed by euthanasia using CO2 (70%) and the tendons were extracted for further evaluation. Our model was adapted from previous evidence and studies[72–74].

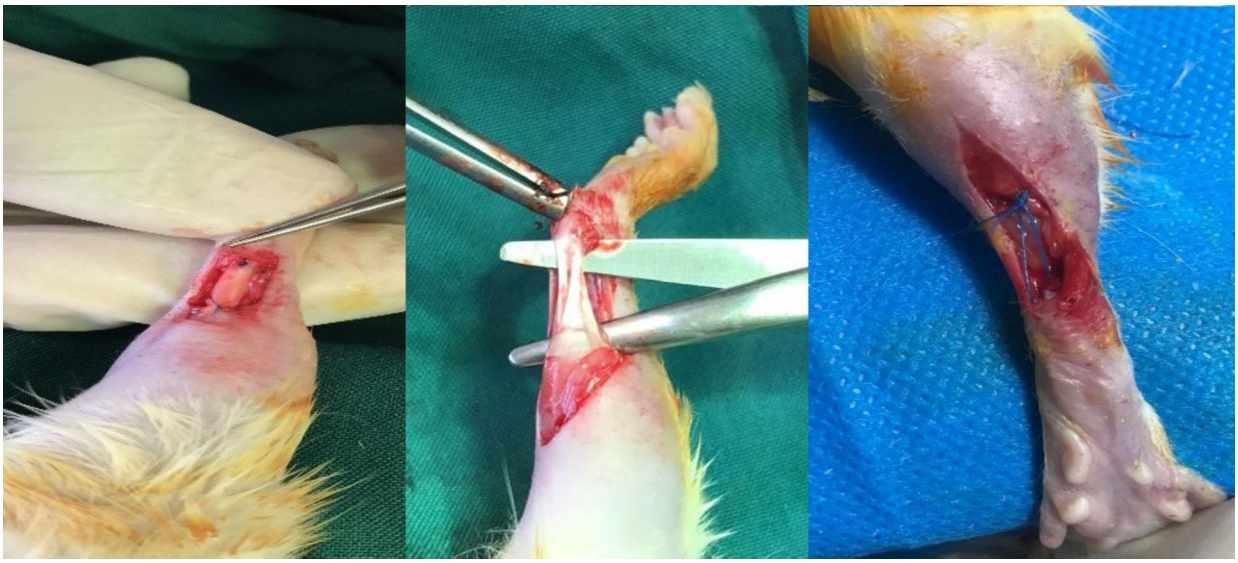

Fig. 1. Implantation and grafting of the scaffold onto the ruptured tendon.

Preparation of PRP

To obtain PRP from the rats, they were anesthetized using an intramuscular injection of xylazine (8 mg/kg) and ketamine HCl (90 mg/kg). Subsequently, the rats underwent jugular vein cannulation. A volume of 3.15 ml of blood was collected from each animal using a 5 ml syringe containing 0.35 ml of 10% sodium citrate. The collected blood was transferred to 5 ml silicone vacuum tubes. Following blood collection, an equal volume of sterile saline was injected into the animals. The blood from each rat was centrifuged at 22 °C for 20 min. The upper fraction, corresponding to the plasma, was then transferred to separate 5 ml silicone vacuum tubes. After further centrifugation of the plasma for 15 min, the lower fraction, containing the PRP, was obtained. The PRP profile included the following parameters: WBC: $0.5 \times 10^3/\mu L$, RBC: $0.04 \times 10^6/\mu L$, Hemoglobin: 0.2 g/dL, platelet: $1180 \times 10^3/\mu L$.

SEM assay

To evaluate the morphology of the repaired AT, the tendons were observed using SEM (TESCAN-Vega 3, Czech Republic). To prepare the samples, they were rinsed in distilled water three times, fixed with 2.5% EM-grade glutaraldehyde for one hour, and triple-rinsed in distilled water. The samples were bisected and dehydrated using graded ethanol. To minimize charging effects, the AT samples were sputter-coated with gold palladium for 120 s. Subsequently, they were examined under SEM at various magnifications.

Histopathologic assay

For histological analysis, the animals were euthanized using CO_2 (75%). The ATs were excised and placed in 10% formalin solution for 72 h. After dehydration with ethanol, the specimens were embedded in paraffin and longitudinally bisected. The sections were stained with hematoxylin–eosin (H&E), and microscopic images were captured using an Olympus microscope (model BX53F, Japan). The specimens were evaluated for inflammatory responses, edema or calcification in the paratendon, collagen fibrils, and neovascularization based on the Backman method[75].

RNA isolation and real-time PCR analysis

Total RNA was isolated from the AT tissue using an RNA extraction kit (FavorPrep Tissue Total RNA Mini Kit, TAIWAN). The purity, integrity, and concentration of RNA were assessed by measuring the optical density at 260/280 nm using a Nanodrop spectrophotometer (Thermo Fisher Scientific, Wilmington, DE, USA). The isolated RNA was then stored at −80 °C until further processing for Complementary DNA (cDNA) synthesis and agarose gel (1%) electrophoresis. cDNA was synthesized from 1 µg of RNA using the RevertAid First Strand cDNA Synthesis Kit (Fermentas Inc.). Real-time PCR was conducted following the protocol of RealQ Plus 2× Master Mix Green (Ampliqon Inc.) in an Applied Biosystems StepOne Instrument (ABI, Step One, USA). For each reaction, 200 nM of specific primers targeting the sequences of interest were added (see Table 1 for primer details). The specific primers targeted genes including collagen type I alpha 1 chain (Col1a1), collagen type III alpha 1 chain (Col3a1), basic fibroblast growth factor (bFGF), Scleraxis (Scx), bHLH transcription factor, and tenomodulin. Additionally, the β2 microglobulin (B2M) housekeeping gene was used as an internal control for real-time PCR reactions. The real-time PCR conditions were set for 10 min at 94 °C, followed by 40 cycles of 15 s at 94 °C, 60 s at 60 °C and extension steps. Following each real-time PCR run, gel electrophoresis and melting curve analysis were performed to confirm the specific amplification of targets. The amplification signals of different samples were normalized to the cycle threshold (Ct) values of B2M, and the delta-delta Ct (2-ΔΔCT) method was employed to compare the mRNA levels of test samples versus controls. The results were expressed as fold changes in data analysis[76].

Genes	Primer sequences	Sizes (bp)
B2m	Forward: 5′-CGTGCTTGCCATTCAGAAA-3′	244
	Reverse: 5′-ATATACATCGGTCTCGGTGG-3′	
Col1a1	Forward: 5′-CTGCCCTCCTGACGCATGG-3′	151
	Reverse: 5′-CATAGCACGCCATCGCACAC-3′	
Col3a1	Forward: 5′-TGGTGGCTTTCAGTTCAGCTA-3′	157
	Reverse: 5′-ATTGCCATTGGCCTGATCCA-3′	
bFGF	Forward: 5′-GCGGCTCTACTGCAAGAA-3′	209
	Reverse: 5′-CTTCTGTAACACACTTAGAAGCC-3′	
Scleraxis (Scx)	Forward: 5′-CAACCAGAGAAAGTTGAGCAAAGA-3′	295
	Reverse: 5′-CATGGAAAGTTCCAGTGGGC-3′	
Tenomodulin	Forward: 5′-TCCCACTCTAATAGCAGTTTCAGA-3′	169
	Reverse: 5′-AAGGTCTTCCTCGCTTGCTT-3′	

Table 1. List of utilized primers in the study. *bp* base pair, *Col1a1* collagen type I alpha 1 chain, *Col3a1* collagen type III alpha 1 chain, *bFGF* basic fibroblast growth factor, *Scx* Scleraxis bHLH transcription factor.

Statistical analysis

All data were recorded and prepared in Microsoft Excel and subsequently analyzed using the Statistical Package for the Social Sciences (SPSS) software, version 26. Student's *t*-test analysis and analysis of variance (ANOVA) test were conducted to assess statistical significance. Additionally, the Mann–Whitney *U* test was employed to compare the group medians of histopathologic results. For the real-time PCR results, data were expressed as the mean ± standard error of the mean (SEM) and analyzed using GraphPad Prism 8 software (GraphPad Software, Inc., La Jolla, CA, USA). A statistically significant value was determined based on a significance level of $P < 0.05$.

Results

Morphology of ostrich ESM

The SEM images of the cross-section of the ESM were captured to assess the morphology of the ESM. As depicted in Fig. 2, the ESM fibers exhibited a random orientation and were not aligned in a specific direction. These fibers were observed to occupy different planes, forming a cross-weave pattern within the ESM. Analysis of the fibers' diameter revealed an average diameter of 2.49 ± 0.89 µm. The distribution of fiber diameters, illustrated in Fig. 2D through a Box and Whisker plot, demonstrated variability in thickness among the fibers. This variability

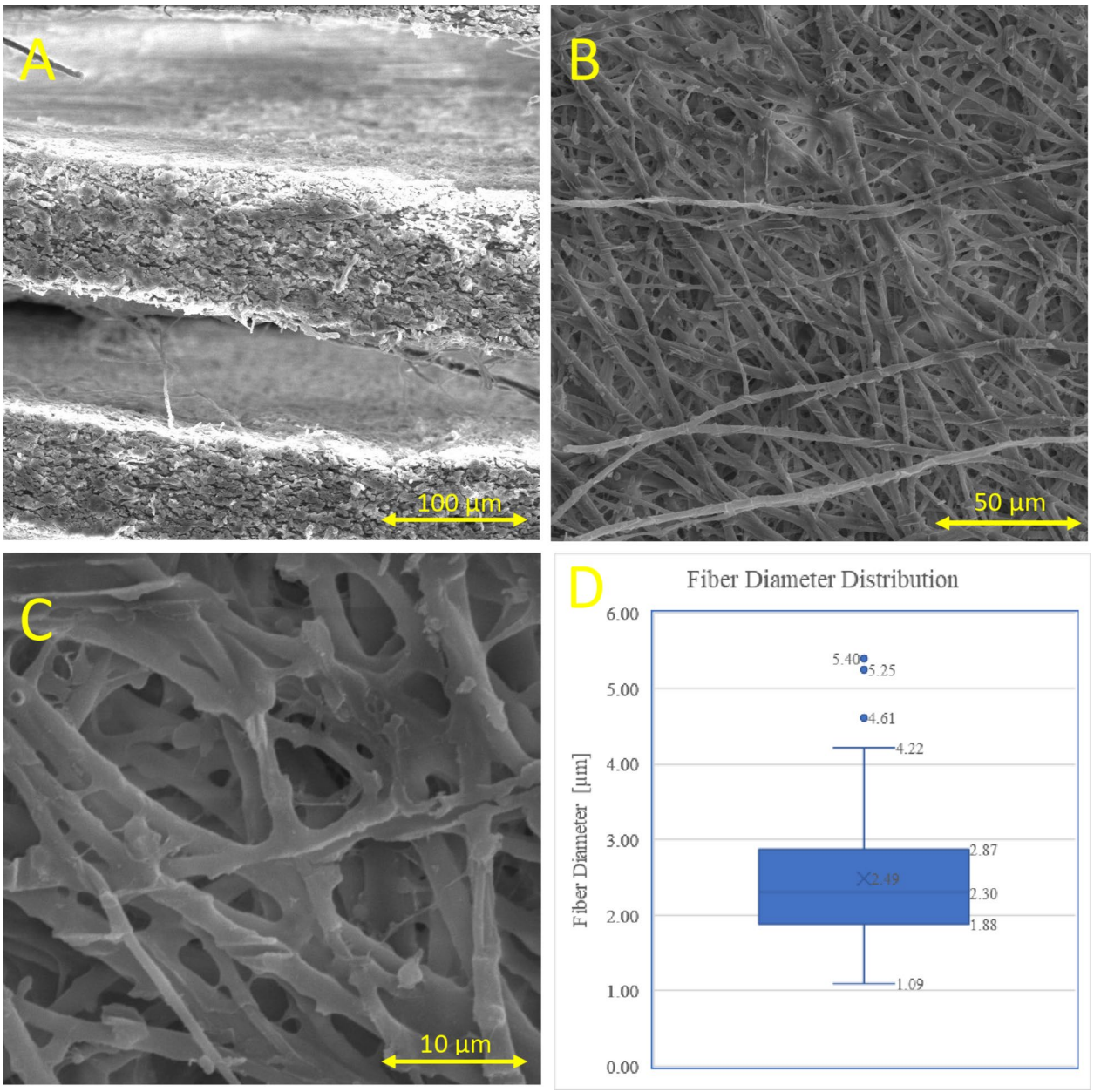

Fig. 2. Scanning electron microscopy images of the ostrich eggshell membrane. Yellow arrows show the scale bar. Magnification of images are (**A**) ×500; (**B**) ×1000; (**C**) ×5000; (**D**) Box and Whisker plot of the ESM fiber diameters, $n = 100$.

in thickness can be attributed to the tendency of the fibers to merge, as evidenced by the SEM images of the ESM surface (Fig. 2A–C).

In vitro biocompatibility

To evaluate the cell viability of the ESM, the MTT assay was employed to assess both the cytotoxicity of the ESM and its capacity to proliferate cell growth (Fig. 3A–E). As depicted in Fig. 3A, the cell survival assessment was conducted on days 3 and 6 following cell culture. The cell viability percentages of the ESM scaffold were determined to be 84.77 ± 3.74 and 94.51 ± 1.50 on days 3 and 6, respectively. According to the literature, cell viability exceeding 80% is considered indicative of biocompatibility[71]. Therefore, the MTT assay results indicated that the ESM scaffolds were non-toxic to the mesenchymal stem cell lines. Additionally, the ESM demonstrated a slight promotion of cell growth from the 3rd day to the 6th day.

In addition to the MTT assay, cellular growth and proliferation were observed using light microscopy and SEM with DAPI staining. As depicted in Fig. 3B, C, cells loaded onto the ESM scaffolds were viable after 3 and 6 days. These images also revealed a slight increase in cell proliferation facilitated by the scaffold.

In vivo biocompatibility

To better understand the biological response to the ESM membrane, an in vivo biocompatibility assay was conducted. Eighteen male Wistar rats were utilized to assess the biocompatibility of the ESM at 7-, 28-, and 56-days post-implantation of the scaffolds. Images representing the implantation site and histopathological assessment of tissues using H&E staining are presented in Fig. 4. Macroscopic evaluation of the implanted site revealed that during the initial week, chronic inflammation was observed at the site of implantation. However, this inflammatory response gradually diminished over time, with inflammation decreasing significantly four weeks post-surgery (Fig. $4B_1$). By the end of 8 weeks, there were no significant signs of inflammation in response to ESM implantation into the body (Fig. $4C_1$–C_3). H&E staining of tissues corroborated these findings. As depicted in Fig. $4A_1$–A_3, at 7 days post-surgery, the implantation site exhibited moderate chronic inflammatory cell infiltration and foreign body type giant cell reaction (*) around the membrane (arrow). By four weeks post-surgery, the tissue displayed mild chronic inflammatory cell infiltration without foreign body type giant cell reaction (Fig. $4B_1$,B_2). Finally, at 56 days post-implantation, tissue sections showed no inflammatory response, neither chronic inflammation nor giant cell reaction (Fig. $4B_1$–B_3).

In vivo model of Achilles tendinopathy

Gait and posture evaluation

The ESM was grafted onto the ruptured AT of rats to assess its potential for tendon tissue recovery. Fourteen weeks post-surgery, the gait behavior of rats was examined to evaluate the recovered AT. The results of stride length and step length of the treated rats at 14 weeks post-surgery are presented in Fig. 5. It was observed that the stride length was higher in all treatment groups compared to the negative control group (CN). However, the SC treatment group showed no significant improvement in stride and step length (Fig. 5). Conversely, the treatment groups receiving scaffolds combined with PRP (either self (SS) or non-self (SP)) exhibited superior results compared to both the negative control group and the treatment group using only ESM scaffolds.

Morphology and histopathological analysis

The H&E images of the tendons in the groups receiving the ESM scaffold (SC) and the ESM scaffold combined with PRP (SP) were captured and compared with those of the negative control group (CN) and the positive control group (CP). Additionally, SEM images of both treated and untreated groups were obtained to assess the effect of the ESM scaffold and ESM combined with PRP on tendon fiber formation (Fig. 6).

The SEM images of the normal tendons (CP) revealed organized fiber alignment and a clear distinction between collagen fibrils and fibers (Fig. 6 CP_{S1}, CP_{S2}). As depicted in Fig. 6 CP_{S1} and CP_{S2}, the fibers in the CP group formed a dense network through interweaving.

In contrast, the untreated control group (CN) displayed not well-organized fibers with low collagen fibril to fiber differentiation (Fig. 6 CN_{S1}, CN_{S2}). Grafting the ESM onto the tendon site improved collagen fibril to fiber differentiation, although fiber organization remained suboptimal in this group (Fig. 6 SC_{S1}, SC_{S2}). Lastly, as shown in Fig. 6 SP_{S1}, SP_{S2}, the combination of ESM with PRP enhanced collagen fibril differentiation and promoted better fiber alignment along the tendon axis. Overall, SEM images indicated that tendon fibers in the SP group exhibited superior alignment and increased fiber differentiation compared to the CN and SC groups.

The H&E staining of the tendon tissue in the normal group (CP) revealed dense, regular, and organized collagen bundles within the connective tissue part of the tendon (Fig. 6 CP_{H1}, CP_{H2}). Notably, the tendon tissue exhibited a characteristic crimp pattern, where nuclei and cytoplasm formed a sinusoidal wave, as observed in Fig. 6 CP_{S1}, CP_{S2}. Minimal neutrophil presence in the histological images indicated an absence of inflammatory response in this group. Furthermore, there was no evidence of edema or calcification in the paratendon tissue.

In contrast, the negative control group (CN) exhibited disorganized collagen bundles within the tendon tissue, consistent with findings from SEM images. Moderate and chronic inflammation was highlighted by the presence of neutrophils in Fig. 6 CN_{H1}, CN_{H2}.

For the SC group, where the ESM was grafted onto the ruptured tendon, histopathological analysis revealed relatively disorganized collagen bundles at the tendon site. Additionally, extensive calcification deposition was observed in the paratendon site, accompanied by mild inflammation indicated by neutrophil presence (Fig. 6 SC_{H1}, SC_{H2}). However, the addition of PRP to the ESM in the SP treatment group inhibited calcium deposition within the tendon tissue. As depicted in Fig. 6 SP_{H1}, SP_{H2}, there was no evidence of calcification deposition, and collagen bundles appeared well-organized in this group.

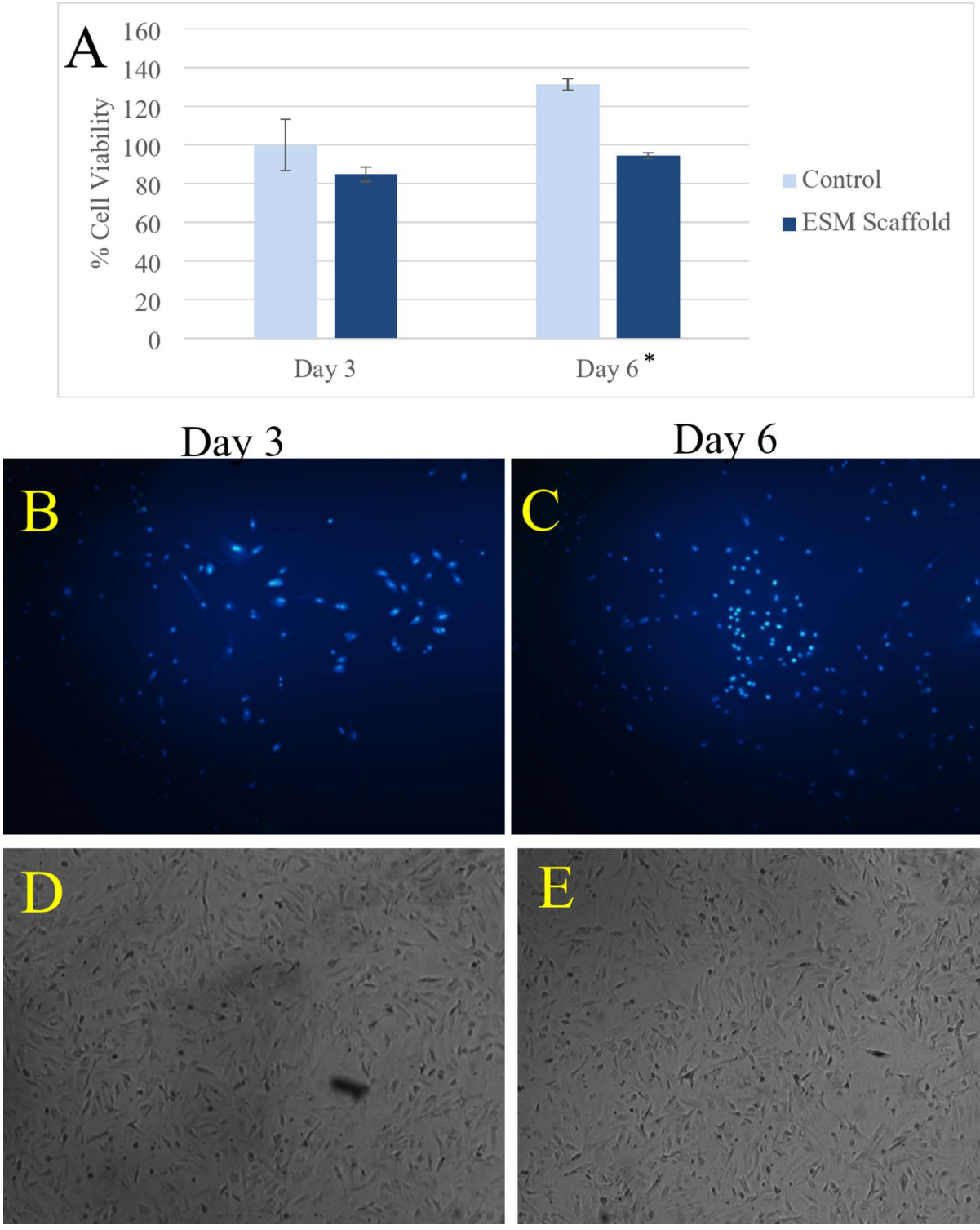

Fig. 3. The results of the cell viability assay of the eggshell membrane. (**A**) The cell viability percentages in days 3 and 6 after cell culture. * Indicates a P-value < 0.05; (**B**) The light microscopy images of the DAPI-stained viable cells in the 3rd day post-culture; (**C**) The light microscopy images of the DAPI-stained viable cells in the 6th day post-culture; (**D**) The SEM images of the DAPI-stained viable cells in the 3rd day post-culture; (**E**) The SEM images of the DAPI-stained viable cells in the 6th day post-culture.

Tensile strength

The mechanical strength of the treated tendons was evaluated using stress-strain assays performed 14 weeks after surgery. The results are presented in Table 2. Normal tendons exhibited a high Young's modulus of 71.01 ± 10.75 MPa and an ultimate strength of 46.75 ± 4.59 N. In comparison, the SC group (Scaffold) showed

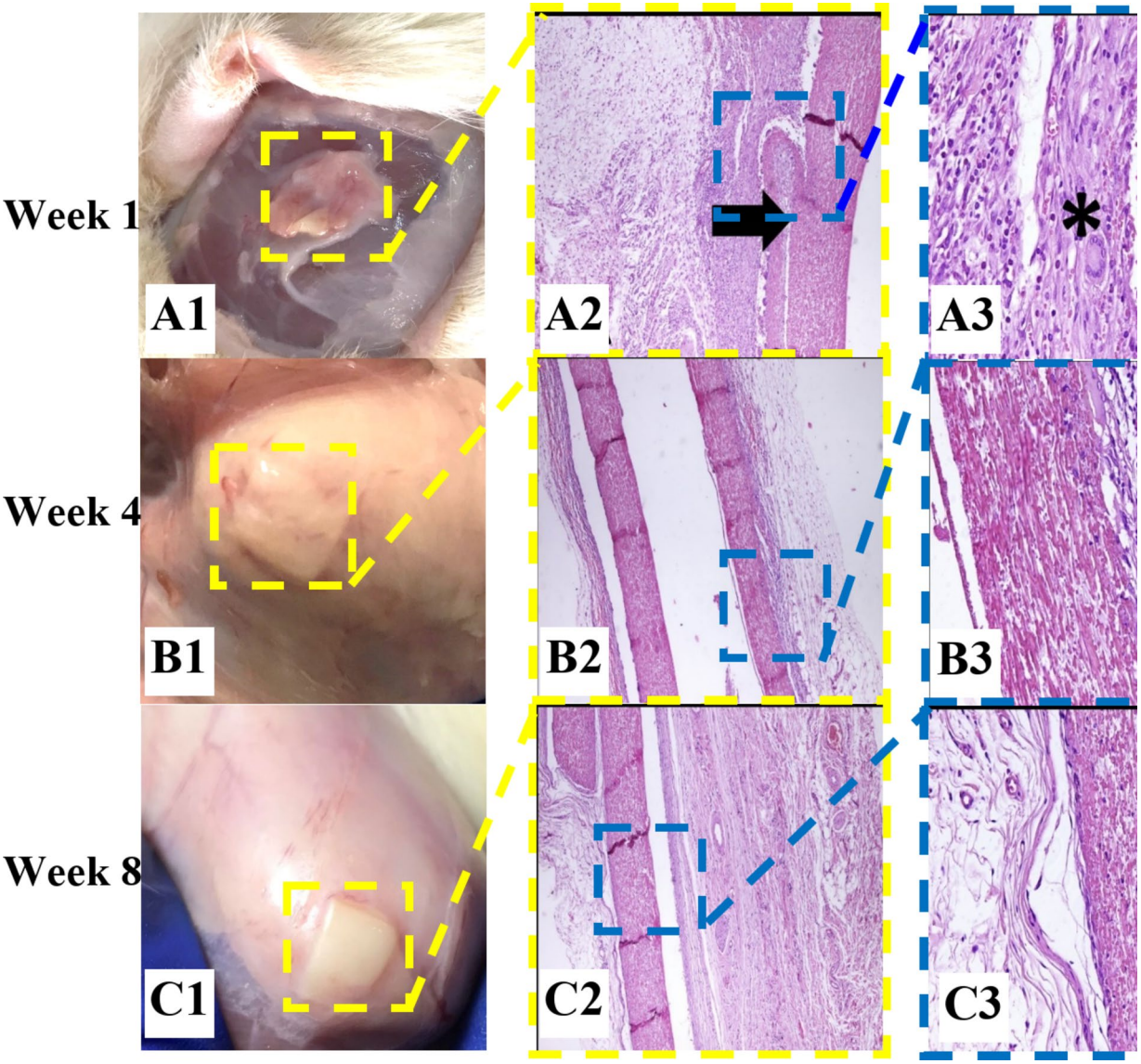

Fig. 4. Histopathological evaluation of bioavailability of ostrich eggshell membrane over time. (**A: A1**) Macroscopic image of the implanted site 7 days post-surgery; (**A2**, **A3**) Histopathological images of the implanted site 7 days after implantation, with magnifications of ×40 and ×200, respectively. These images depict moderate chronic inflammatory cell infiltration and foreign body type giant cell reaction (*) around the membrane (arrow). (**B**: **B1**) Macroscopic image of the implanted site 4 weeks post-surgery; (**B2**, **B3**) Histopathological images of the implanted site 4 weeks after implantation, with magnifications of ×40 and ×200, respectively. These sections show mild chronic inflammatory cell infiltration without foreign body type giant cell reaction. (**C**: **C1**) Macroscopic image of the implanted site 8 weeks post-surgery; (**C2**, **C3**) Histopathological images of the implanted site 8 weeks after implantation, with magnifications of ×40 and ×200, respectively. These sections demonstrate no inflammatory response, neither chronic inflammation nor giant cell reaction.

a Young's modulus of 15.27 ± 4.41 MPa and an ultimate strength of 41.42 ± 14.90 N. Meanwhile, the SP group (Scaffold + PRP) exhibited an ultimate strength of 48.91 ± 15.56 N and a Young's modulus of 20.90 ± 7.53 MPa. However, the differences in the data were not statistically significant (P-Value > 0.05).

Gene expression

The gene expression analysis related to tendon regeneration and tenogenesis reveals that the surgical tissue exhibits high expression levels of Col1a1, Col3a1, bFGF, Scx, and tenomodulin, all crucial for the structural organization of the tendon. In comparison to the CP (control) group, the CN group exhibits a significant decrease in all genes ($P < 0.05$). However, both the SS (1.27-fold, $P = 0.008$) and SP (1.49-fold, $P = 0.003$) groups show a significant up-regulation in the expression of Col1a1 compared to the CN group (0.31-fold). Additionally, the Col3a1 gene expression is increased in the SC (0.78-fold, $P = 0.019$), SS (2.14-fold, $P < 0.001$), and SP (2.07-

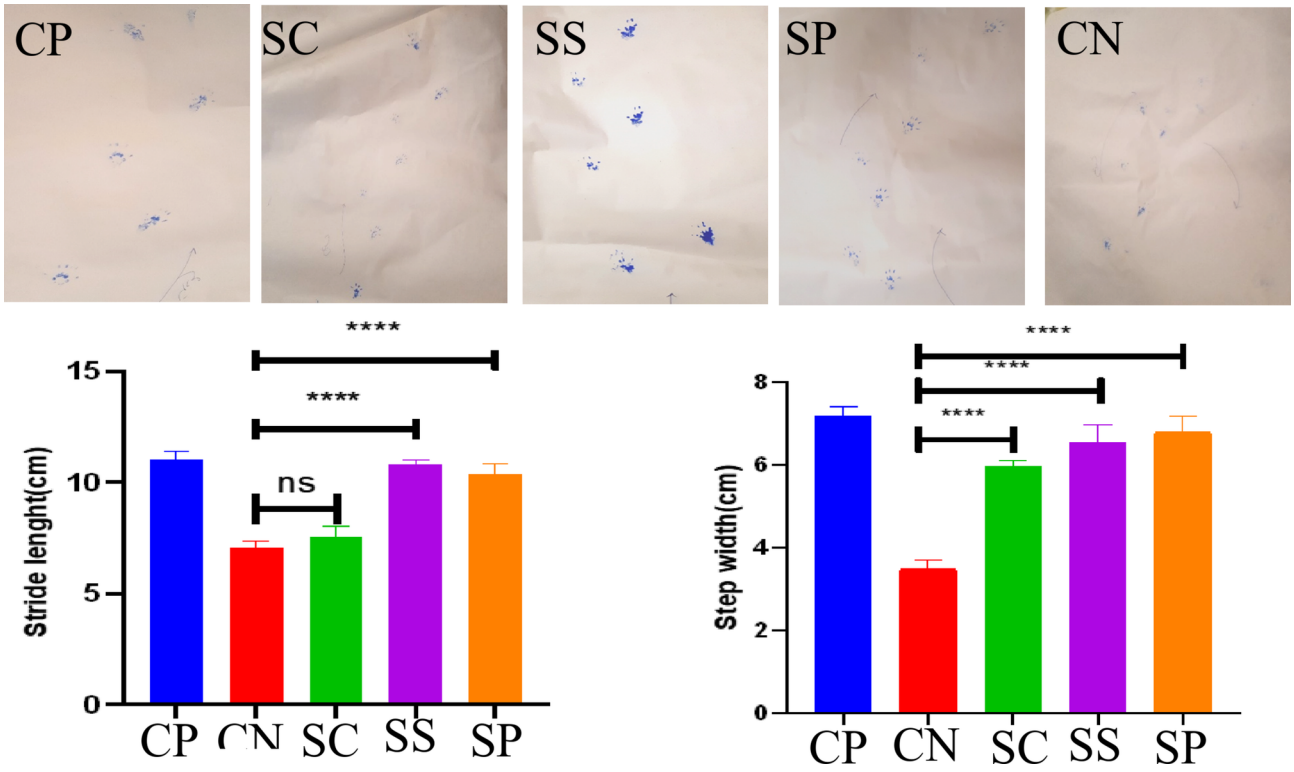

Fig. 5. Gait analysis of rats 14 weeks post-surgery; *CP* Positive control group, where rats had normal tendons; *CN* Negative control group, where rats with Achilles tendinopathy received no treatment; *SC* Treatment group, where Ostrich eggshell membrane was grafted to the ruptured Achilles tendon; *SP* Treatment group, where Ostrich eggshell membrane combined with platelet-rich plasma was grafted to the ruptured Achilles tendon; ***P-value < 0.05; *ns* not statistically significant.

fold, $P < 0.001$) groups compared to the CN group (0.42-fold). Analysis of bFGF, Scx, and tenomodulin gene expression reveals a similar upward trend in the SS (1.17, 0.65, and 0.68, respectively) and SP (0.89, 0.53, and 0.82, respectively) groups compared to the CN group (0.21, 0.08, and 0.15, respectively) ($P < 0.05$) (Fig. 7).

Discussion

The study investigated Ostrich ESM as a scaffold for AT regeneration. Our findings demonstrate that the combination of Ostrich ESM with PRP significantly enhances AT repair and is a biocompatible scaffold for the application in living organisms. In vitro tests showed no toxicity to cells, and in vivo implantation in rats demonstrated safety over 8 weeks. Combining ESM with PRP in an Achilles tendinopathy model regenerated tendon tissue within 14 weeks, supported by various analyses. Previous research has predominantly employed synthetic scaffolds for tendon repair. Webb et al. utilized poly(3-hydroxybutyrate-co-3-hydroxyhexanoate) (PHBHHx) combined with collagen and tenocytes to create a scaffold for Achilles tendinopathy treatment in an in vivo rat model, which highlighted collagen's role in treating tendon injuries[77]. Sun et al. prepared a functional collagen scaffold tethered with recombinant SDF-1a (CBD-SDF-1a) for rat AT defect regeneration. The scaffold increased CXCR4-positive fibroblast-like cell recruitment and Tenascin-C deposition at 7 days. At 4 and 12 weeks, it enhanced type I collagen expression, collagen fibril diameter, and tendon mechanical properties. This scaffold facilitates tendon regeneration by regulating SDF-1a release, enhancing cell recruitment, and providing a supportive microenvironment[78]. Furthermore, Gabler et al. introduced a bovine cross-linked collagen scaffold for treating AT defects in an in vivo rat model; however, they encountered a high failure rate of 48%, primarily attributable to suture tear-out from the tendon[79]. Our study is the first to assess the biocompatibility of the Ostrich ESM scaffold in an in vivo AT model, yielding satisfactory in vivo and in vitro outcomes.

Regarding the morphology of Ostrich ESM, previous studies have also reported similar findings using different microscopy techniques. Richards et al. reported an average diameter of 2.8 ± 1 µm for ostrich ESM fibers using light microscopy. Furthermore, both this study and previous research have indicated that the ESM fibers are rich in type I collagen and contain minerals such as calcium, sulfur, and magnesium[80,81].

We evaluated the in vitro biocompatibility of ostrich ESM for further application in living organism. By conducting the MTT assay and considering cell viability exceeding 80% as indicative of biocompatibility, we found that the ESM scaffolds did not exhibit toxicity towards the mesenchymal stem cell lines[71]. This observed cell growth can be attributed to the collagenous structure of the ESM fibers, which facilitated cellular proliferation[82]. However, the modest rate of cell proliferation may be attributed to insufficient time for extensive cell growth. This finding is consistent with a previous study conducted by Choi et al. in 2020[83], which evaluated the MTT

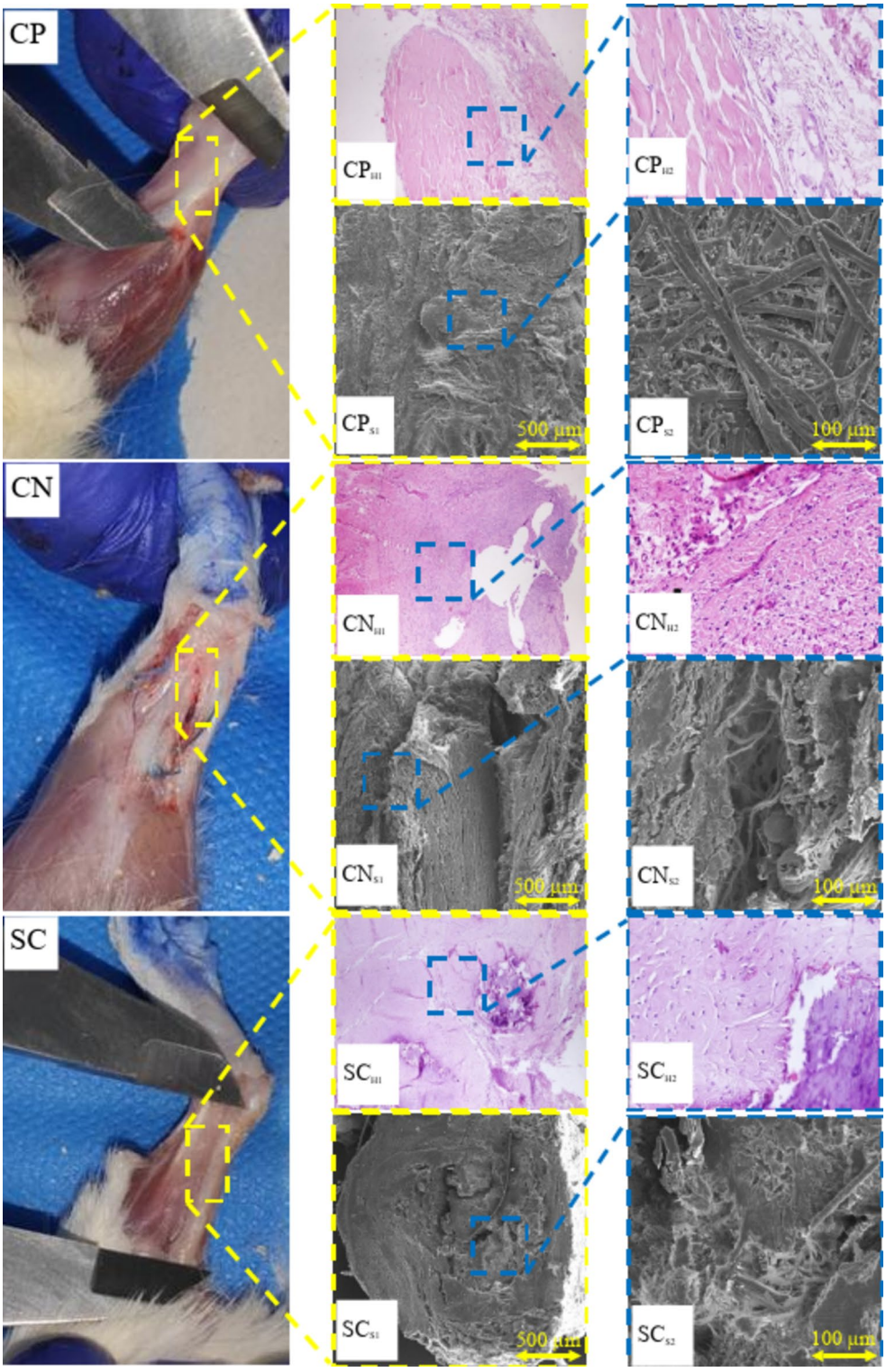

Fig. 6. Histological and scanning electron microscopy (SEM) evaluation of tendon regeneration with Ostrich eggshell membrane (ESM) and platelet-rich plasma (PRP) treatment. H&E staining images of tendon tissue from the negative control (CN), positive control (CP), Ostrich ESM scaffold (SC), and Ostrich ESM scaffold combined with PRP (SP) groups are compared. SEM images depict the morphology of tendon fibers in each group. Normal tendons (CP) display organized fiber alignment and dense collagen fibrils (CP_{H1}, CP_{H2}). In contrast, CN group exhibits disorganized collagen bundles and signs of inflammation (CN_{H1}, CN_{H2}). SC group shows improved collagen fibril differentiation but disorganized fibers (SC_{S1}, SC_{S2}). SP group demonstrates enhanced collagen fibril differentiation and aligned fibers (SP_{S1}, SP_{S2}), with reduced inflammation and calcification (SP_{H1}, SP_{H2}).

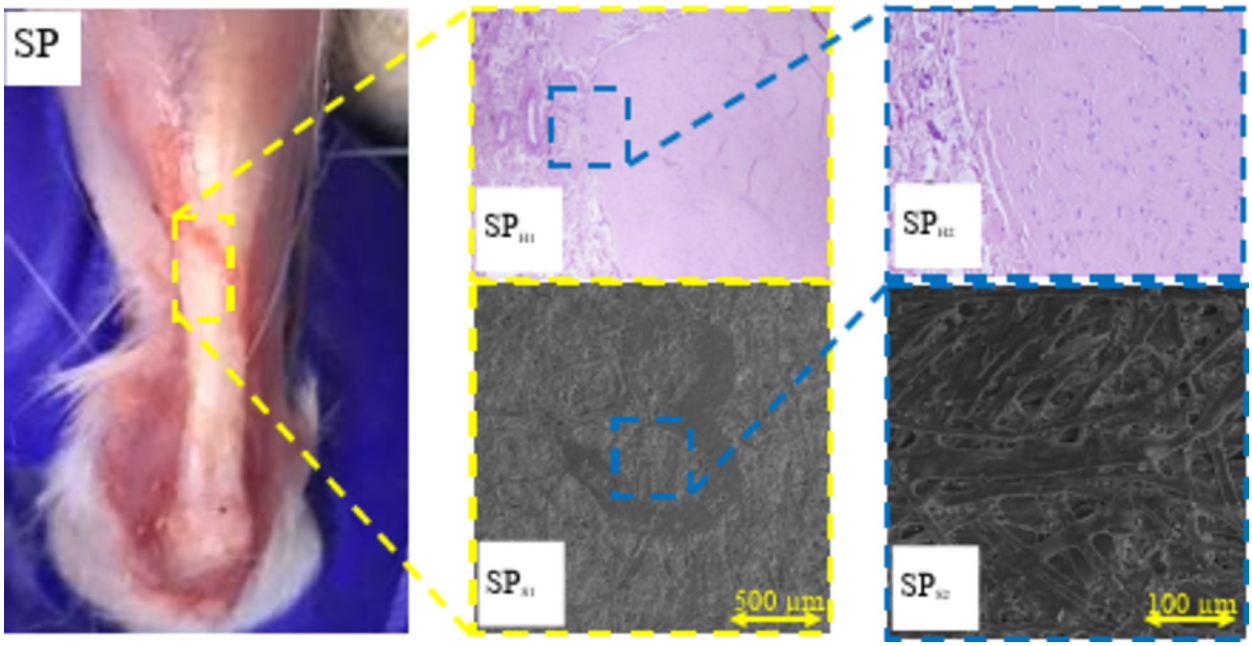

Figure 6. (continued)

Group	Young's modulus (MPa)	Ultimate strength (*N*)
Positive control	71.01 ± 10.75	46.75 ± 4.59
SC (Scaffold)	15.27 ± 4.41	41.42 ± 14.90
SP (Scaffold + Platelet-Rich Plasma)	20.90 ± 7.53	48.91 ± 15.56

Table 2. Mechanical strength evaluation of treated tendons 14 weeks post-surgery. Young's modulus and ultimate strength are presented for the positive control group (normal tendons), the treatment group using scaffold only (SC), and the treatment group using scaffold combined with platelet-rich plasma (SP). Data are expressed as mean ± standard deviation.

assay of chicken ESM on days 1, 7, 14, and 28 post-cell culture. They reported that significant proliferation was not observed until the 7th day, after which the proliferation rate sharply increased[83]. Another study assessed the proliferation of human dermal fibroblast cells in the presence of chicken ESM and demonstrated that chicken ESM has the potential to promote cell growth[84]. Overall, it can be concluded that ostrich ESM exhibited no significant toxicity to mesenchymal stem cells and could support cellular proliferation.

In addition to the MTT assay, cellular growth and proliferation were observed using light microscopy and SEM with DAPI staining. As depicted in Fig. 3B, C, cells loaded onto the ESM scaffolds were viable after 3 and 6 days. These images also revealed a slight increase in cell proliferation facilitated by the scaffold. The interwoven and fibrous structure of the ESM can provide physical support for cell adhesion and growth[85]. Moreover, the high collagen content, presence of glycoproteins, and minerals in ostrich ESM could further enhance cellular proliferation[86]. In a study by Gharibi and Abdolmaleki, the MG-63 cell line was cultured on neat chicken ESM and chicken ESM modified with citric acid. They found that the modified ESM with citric acid exhibited superior results due to the more aligned fiber morphology[86]. Therefore, the relatively low proliferation rate of cells loaded onto the ESM in the early days after cell culture may be associated with the non-aligned fibrous structure of the ESM, as evidenced by SEM images of the ESM scaffolds.

Studies have primarily focused on evaluating the in vitro biocompatibility of Avian ESM, with few reporting on in vivo biocompatibility. As demonstrated in the MTT assay, Ostrich ESM was found to be non-toxic to mesenchymal stem cells and promoted cellular growth and proliferation over time. Previous studies have also indicated that ESM can enhance cellular growth in various cell lines, including human dermal fibroblast cells, MG-63, and hemopoietin stem cells[84,86,87]. The in vivo biocompatibility assay in our study revealed that Ostrich ESM mitigated the inflammatory response over time. This finding aligns with a study by Vuong et al., where they investigated the anti-inflammatory effect of ESM on lipopolysaccharide-induced inflammatory U937–3xκB-LUC cells[88]. According to their study, ESM inhibited the activity of the transcription factor nuclear factor-κB and increased the secretion of the anti-inflammatory cytokine IL-10, thereby reducing inflammation[88]. Overall, it is concluded that ESM can attenuate the inflammatory response of the body and is safe for in vivo applications.

We further aimed to evaluate our finding in a in vivo model of Achilles Tendinopathy. The combination of Ostrich ESM with PRP showed promise in enhancing rat gait after 14 weeks, suggesting its potential efficacy

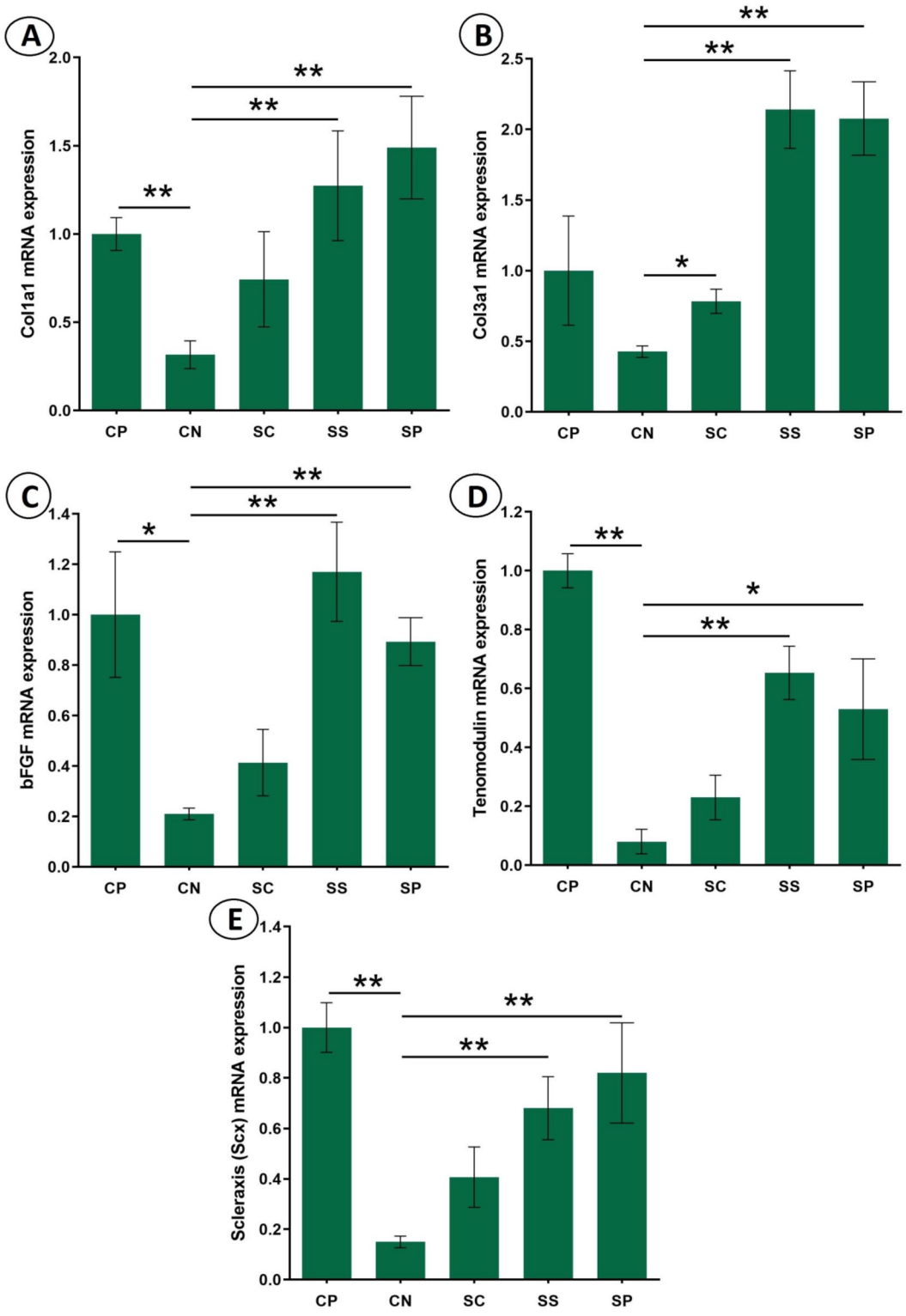

Fig. 7. Impact of double-layered Ostrich eggshell membrane (ESM) and platelet-rich plasma (PRP) on the gene expression related to tendon regeneration. The control negative (CN) group served as the control, where Achilles tendon rupture was induced without treatment. mRNA levels of Col1a1, Col3a1, bFGF, Scleraxis (Scx), and tenomodulin were quantified using real-time PCR in different groups; (**A**) The mRNA expression analysis for Col1a1 gene expression level; (**B**) Effect of ESM and PRP on Col3a1 expression in the groups; (**C**) bFGF mRNA expression levels in the groups; (**D**) Scleraxis (Scx) gene expression after the effect of ESM and PRP on tendon tissue; (**E**) The mRNA expression analysis for tenomodulin gene expression level. Expression data, relative to those of the reference gene, from at least three independent assays are presented as mean ± SEM. Statistical significance was tested using one-way ANOVA. * denotes P value < 0.05; ** denotes P value < 0.01.

in tendon recovery. This finding suggests that PRP played a significant role in the healing of the ruptured AT. Previous studies have also highlighted the significant role of PRP in AT treatment. For instance, Circi et al. evaluated the effect of PRP injection at different time intervals on Achilles tendinopathy treatment in a rat model. Their results demonstrated that immediate PRP injection at the injured site significantly enhanced tendon healing in rats[89]. Similarly, in a study by Parafirioti et al., eighty male rats were used to assess the impact of PRP injection on AT regeneration. The study concluded that a single PRP injection at the ruptured site facilitated injured tendon regeneration within the first week of treatment[90].

Furthermore, the histopathological evaluation and SEM images demonstrated that the addition of PRP to the Ostrich ESM scaffold facilitated tendon tissue regeneration. The Ostrich ESM scaffold promoted fiber differentiation compared to the negative control (CN) group, albeit with signs of calcification in that group. The presence of calcium in the tendon tissue might be attributed to specific features of ESM, such as its morphology and structure. Previous studies have suggested that ESM is an appropriate site for the mammillary knobs where the nucleation of calcium carbonate crystals occur[91,92]. In contrast, the addition of PRP to the ESM scaffolds enhanced collagen fibril-to-fiber differentiation and resulted in more aligned fibers. PRP contains various growth factors like transforming growth factor-b1, insulin-like growth factors 1 and 2, vascular endothelial growth factor (VEGF), basic fibroblast growth factor, and hepatocyte growth factor (HGF), which promote cellular adhesion and induce fibroblast production, ultimately improving collagen synthesis and organization[65,93]. Overall, the combination of ESM and PRP facilitated better reformation of tendon fibers compared to the negative control group and the treatment group using only ESM scaffolds.

Regarding tensile strength, the treatment group receiving the ESM scaffold exhibited the lowest Young's modulus. As previously mentioned, this treatment tended to result in the deposition of calcification in the tendon tissues. The low Young's modulus observed in this group can be attributed to the accumulation of calcium, which reduces the elasticity of the tendons. Furthermore, the SP group demonstrated higher ultimate strength. The increased ultimate strength in tendons treated with the ESM scaffold combined with PRP is attributed to the well-organized and dense fiber structure of the tendon, as discussed in the Morphology and Histopathology Analysis section. Based on our findings, the elasticity modulus declined in the treatment groups compared to the normal tendons. This result aligns with the findings of a study by Webb et al., where various synthetic scaffolds of PHBHHx, collagen, and tenocytes were used[77]. In a study by Yu et al., a synthetic electrospun scaffold based on poly(lactic-co-glycolic acid) was developed to treat AT injuries. In their study, the ultimate strength obtained for normal tendons and treated tendons were 4.02 ± 4.74 N and 18.32 ± 2.69 N, respectively[94]. These data were significantly lower compared to our derived results. Another study utilized a bovine cross-linked collagen scaffold to regenerate defected AT in rat models. In this study, the ultimate strength of normal tendons was reported to be 76.6 ± 11.6 N, which was more similar to our findings[95]. However, differences in results could be attributed to various factors, such as variations in the average diameters of fibers in the tendon[94].

Overall, the real-time PCR results emphasizes the significance of enhanced tendon formation in both ESM-PRP treatment groups. Gene expression shows a significant high expression of Col1a1, Col3a1, bFGF, Scx and tenomodulin both groups, which has also been reported in previous studies[96,97]. Sugimoto et al. employed a loss-of-function approach to demonstrate that Scx+/Sox9+ progenitors play a functional role in establishing the junction between hyaline cartilage and tendon/ligament tissues[98]. Scx expression is up-regulated during tendon formation, such as in Achilles and patella tendons, as well as in the cruciate ligaments of the knee joint. Conversely, its expression is down-regulated at sites undergoing chondrogenesis. These findings suggest that the coordinated expression of Scx is tightly regulated to specify and maintain tenocyte, chondrocyte, and osteocyte populations[98,99].

Our study has its limitations. CCK-8 and Live-Dead assays are more commonly used to evaluated biocompatibility of a scaffold through in-vitro studies, which was not performed in our study. Although we've demonstrated that the ESM-PRP scaffold enhances fibroblast-like cell recruitment and fosters tendon regeneration, we couldn't identify the proportion of each cell type—mesenchymal stem cells, dermal fibroblasts, and AT fibroblasts—due to the absence of specific markers. Our study also lacks blood and serum test evaluations. We also utilized the RT-qPCR method instead of COL-I and COL-III IHC staining, due to the wider dynamic range and higher sensitivity, and also based on our limited resources[100]. However, COL I/III ratio could have enhanced the validity of our technique, since successful remodeling is characterized by replacement of type III collagen with type I collagen, while the maintenance of high type III collagen expression levels is reportedly associated with scar formation and adhesion rather than normal healing. Further research is necessary to determine which cell types contribute to tendon regeneration.

Conclusion

The present study explored the potential of Ostrich ESM as a natural scaffold for tissue regeneration. In vitro biocompatibility testing revealed no significant toxicity to mesenchymal stromal cells. Implantation of ESM in Wister rats demonstrated its safety for long-term use over 8 weeks. Consequently, ESM was deemed suitable for further investigation in tissue regeneration. In an in vivo Achilles tendinopathy model, combining ESM with PRP successfully regenerated tendon tissue within 14 weeks. This conclusion was supported by gait analysis, histopathology, and tensile strength assays, and gene expression of treated tendons. Future studies may explore combining ESM with other materials to enhance mechanical strength and biological efficiency.

Data availability

All data regarding this study has been reported in the manuscript. Please contact the corresponding author if interested in any further information.

Received: 2 May 2024; Accepted: 1 January 2025
Published online: 04 January 2025

References

1. Voleti, P. B., Buckley, M. R. & Soslowsky, L. J. Tendon healing: repair and regeneration. *Annu. Rev. Biomed. Eng.* **14**, 47–71 (2012).
2. Raikin, S. M., Garras, D. N. & Krapchev, P. V. Achilles tendon injuries in a United States population. *Foot Ankle Int.* **34**(4), 475–480 (2013).
3. Jarvinen, T. A., Kannus, P., Maffulli, N. & Khan, K. M. Achilles tendon disorders: etiology and epidemiology. *Foot Ankle Clin.* **10**(2), 255–266 (2005).
4. Arnoczky, S. P. & László, G. Józsa and Pekka Kannus. Champaign, Illinois, Human Kinetics, 1997. $79.00, 573 pp. *J. Bone Joint Surg.* **81**(1), 148 (1999).
5. Jarvinen, M. Epidemiology of tendon injuries in sports. *Clin. Sports Med.* **11**(3), 493–504 (1992).
6. Maffulli, N. & Kader, D. Tendinopathy of tendo achillis. *J. Bone Joint Surg. Br.* **84**(1), 1–8 (2002).
7. Paavola, M. et al. Achilles tendinopathy. *J. Bone Joint Surg. Am.* **84**(11), 2062–2076 (2002).
8. Johansson, C. Injuries in elite orienteers. *Am. J. Sports Med.* **14**(5), 410–415 (1986).
9. Kvist, M. Achilles tendon injuries in athletes. *Sports Med.* **18**(3), 173–201 (1994).
10. Leppilahti, J., Karpakka, J., Gorra, A., Puranen, J. & Orava, S. Surgical treatment of overuse injuries to the Achilles tendon. *Clin. J. Sport Med.* **4**(2), 100–107 (1994).
11. Schonbauer, H. R. Diseases of the Achilles tendon. *Wien Klin. Wochenschr Suppl.* **168**, 1–47 (1986).
12. Jarvinen, T. A., Jarvinen, T. L., Kannus, P., Jozsa, L. & Jarvinen, M. Collagen fibres of the spontaneously ruptured human tendons display decreased thickness and crimp angle. *J. Orthop. Res.* **22**(6), 1303–1309 (2004).
13. Kvist, M., Jozsa, L. & Jarvinen, M. Vascular changes in the ruptured Achilles tendon and paratenon. *Int. Orthop.* **16**(4), 377–382 (1992).
14. Tallon, C., Maffulli, N. & Ewen, S. W. Ruptured Achilles tendons are significantly more degenerated than tendinopathic tendons. *Med. Sci. Sports Exerc.* **33**(12), 1983–1990 (2001).
15. Lonzarić, D., Kruščić, A., Dinevski, D., Povalej Bržan, P. & Jesenšek Papež, B. Primary surgical repair of acute Achilles tendon rupture: comparative results of three surgical techniques. *Wien. Klin. Wochenschr.* **129**, 176–185 (2017).
16. Sugimoto, K. et al. M9: recent developments in the treatment of ankle and subtalar instability. *Open. Orthop. J.* **11**, 687 (2017).
17. Clark, R. R. et al. Patch augmentation for rotator cuff repair: indications, techniques, and outcomes. *Oper. Tech. Sports Med.* **20**(3), 224–232 (2012).
18. Müller, A. M., Flury, M., Alsayed, H. N. & Audigé, L. Influence of patient and diagnostic parameters on reported retear rates after arthroscopic rotator cuff repair. *Knee Surg. Sports Traumatol. Arthrosc.* **25**, 2089–2099 (2017).
19. Galatz, L. M., Gerstenfeld, L., Heber-Katz, E. & Rodeo, S. A. Tendon regeneration and scar formation: the concept of scarless healing. *J. Orthop. Res.* **33**(6), 823–831 (2015).
20. Eriksen, H. A., Pajala, A., Leppilahti, J. & Risteli, J. Increased content of type III collagen at the rupture site of human Achilles tendon. *J. Orthop. Res.* **20**(6), 1352–1357 (2002).
21. Ochen, Y. et al. Operative treatment versus nonoperative treatment of Achilles tendon ruptures: systematic review and meta-analysis. *BMJ* **364**, k5120 (2019).
22. Lantto, I. et al. A prospective randomized trial comparing surgical and nonsurgical treatments of acute Achilles tendon ruptures. *Am. J. Sports Med.* **44**(9), 2406–2414 (2016).
23. Wilkins, R. & Bisson, L. J. Operative versus nonoperative management of acute Achilles tendon ruptures: a quantitative systematic review of randomized controlled trials. *Am. J. Sports Med.* **40**(9), 2154–2160 (2012).
24. Aktas, E. et al. Immune modulation with primed mesenchymal stem cells delivered via biodegradable scaffold to repair an Achilles tendon segmental defect. *J. Orthop. Res.* **35**(2), 269–280 (2017).
25. Liu, Y., Ramanath, H. S. & Wang, D. A. Tendon tissue engineering using scaffold enhancing strategies. *Trends Biotechnol.* **26**(4), 201–209 (2008).
26. Wu, G., Deng, X., Song, J. & Chen, F. Enhanced biological properties of biomimetic apatite fabricated polycaprolactone/chitosan nanofibrous bio-composite for tendon and ligament regeneration. *J. Photochem. Photobiol. B* **178**, 27–32 (2018).
27. Zhang, C. et al. An epigenetic bioactive composite scaffold with well-aligned nanofibers for functional tendon tissue engineering. *Acta Biomater.* **66**, 141–156 (2018).
28. Langer, R. & Tirrell, D. A. Designing materials for biology and medicine. *Nature* **428**(6982), 487–492 (2004).
29. Place, E. S., Evans, N. D. & Stevens, M. M. Complexity in biomaterials for tissue engineering. *Nat. Mater.* **8**(6), 457–470 (2009).
30. Giannitelli, S. M., Accoto, D., Trombetta, M. & Rainer, A. Current trends in the design of scaffolds for computer-aided tissue engineering. *Acta Biomater.* **10**(2), 580–594 (2014).
31. Zhou, H. & Lee, J. Nanoscale hydroxyapatite particles for bone tissue engineering. *Acta Biomater.* **7**(7), 2769–2781 (2011).
32. İlik, M. B., Durmuş, E. & Çelik, İ. Biocompatibility and osseointegration of the biomimetically coated and water-soluble eggshell membrane protein cross-linked Ti alloy screws. *Iran. Biomed. J.* **28**(1), 38 (2024).
33. Durmuş, E., Celik, I., Ozturk, A., Ozkan, Y. & Aydin, M. Evaluation of the potential beneficial effects of ostrich eggshell combined with eggshell membranes in healing of cranial defects in rabbits. *J. Int. Med. Res.* **31**(3), 223–230 (2003).
34. Muhammed, M. R., Omer, O. A. & Ahmed, B. M. The use of Ostrich eggshell membrane as a barrier for guided bone regeneration in rabbit's femoral condyle defects: histological study. *Int. J. Pharm. Res.* **12**(1), 963–969 (2020).
35. Leal-Marin, S. et al. Human amniotic membrane: a review on tissue engineering, application, and storage. *J. Biomed. Mater. Res. Part. B Appl. Biomater.* **109**(8), 1198–1215 (2021).
36. Park, S. et al. Eggshell membrane: review and impact on engineering. *Biosyst Eng.* **151**, 446–463 (2016).
37. Arias, J. L., Fernandez, M. S., Dennis, J. E. & Caplan, A. I. Collagens of the chicken eggshell membranes. *Connect. Tissue Res.* **26**(1–2), 37–45 (1991).
38. Fernandez, M. S., Araya, M. & Arias, J. L. Eggshells are shaped by a precise spatio-temporal arrangement of sequentially deposited macromolecules. *Matrix Biol.* **16**(1), 13–20 (1997).
39. Harris, E. D., Blount, J. E. & Leach, R. M. Jr. Localization of lysyl oxidase in hen oviduct: implications in egg shell membrane formation and composition. *Science* **208**(4439), 55–56 (1980).
40. Kawakami, H., Yoshida, K., Nishida, Y., Kikuchi, Y. & Sato, Y. Antibacterial properties of metallic elements for alloying evaluated with application of JIS Z 2801:2000. *ISIJ Int.* **48**(9), 1299–1304 (2008).
41. Leach, R. M. Biochemistry of the organic matrix of the eggshell. *Poult. Sci.* **61**(10), 2040–2047 (1982).
42. Nys, Y., Gautron, J., Garcia-Ruiz, J. M. & Hincke, M. T. Avian eggshell mineralization: biochemical and functional characterization of matrix proteins. *C.R. Palevol.* **3**(6–7), 549–562 (2004).
43. Wong, M., Hendrix, M. J., von der Mark, K., Little, C. & Stern, R. Collagen in the egg shell membranes of the hen. *Dev. Biol.* **104**(1), 28–36 (1984).
44. Zhao, Y-H. & Chi, Y-J. Characterization of collagen from eggshell membrane. *Biotechnol. (Faisalabad).* **8**(2), 254–258 (2009).
45. Hincke, M. T. et al. Identification and localization of lysozyme as a component of eggshell membranes and eggshell matrix. *Matrix Biol.* **19**(5), 443–453 (2000).

46. Gautron, J. et al. Ovotransferrin is a matrix protein of the hen eggshell membranes and basal calcified layer. *Connect. Tissue Res.* **42**(4), 255–267 (2001).
47. Hincke, M. T. Ovalbumin is a component of the chicken eggshell matrix. *Connect. Tissue Res.* **31**(3), 227–233 (1995).
48. Cordeiro, C. M., Esmaili, H., Ansah, G. & Hincke, M. T. Ovocalyxin-36 is a pattern recognition protein in chicken eggshell membranes. *PLoS One*. **8**(12), e84112 (2013).
49. Gautron, J. et al. Cloning of ovocalyxin-36, a novel chicken eggshell protein related to lipopolysaccharide-binding proteins, bactericidal permeability-increasing proteins, and plunc family proteins. *J. Biol. Chem.* **282**(8), 5273–5286 (2007).
50. Starcher, B. C. & King, G. S. The presence of desmosine and isodesmosine in eggshell membrane protein. *Connect. Tissue Res.* **8**(1), 53–55 (1980).
51. Nys, Y., Gautron, J., McKee, M. D., Garcia-Ruiz, J. M. & Hincke, M. T. Biochemical and functional characterisation of eggshell matrix proteins in hens. *World's Poult. Sci. J.* **57**(4), 401–413 (2019).
52. Balaz, M. Eggshell membrane biomaterial as a platform for applications in materials science. *Acta Biomater.* **10**(9), 3827–3843 (2014).
53. Gong, W., He, W., Hou, Y., Li, Y. & Hu, J. Tendon-inspired hybrid hydrogel based on polyvinyl alcohol and gallic acid-lysozyme for promoting wound closure and healing. *Int. J. Biol. Macromol.* **247**, 125583 (2023).
54. Tack, C., Shorthouse, F. & Kass, L. The physiological mechanisms of effect of vitamins and amino acids on tendon and muscle healing: a systematic review. *Int. J. Sport Nutr. Exerc. Metab.* **28**(3), 294–311 (2018).
55. Farrar, G., Barone, J. & Morgan, A. Ovalbumin-based porous scaffolds for bone tissue regeneration. *J. Tissue Eng.* **1**(1), 209860 (2010).
56. Marinovich, R. et al. The role of bone sialoprotein in the tendon–bone insertion. *Matrix Biol.* **52**, 325–338 (2016).
57. Cordeiro, C. M. & Hincke, M. T. Quantitative proteomics analysis of eggshell membrane proteins during chick embryonic development. *J. Proteom.* **130**, 11–25 (2016).
58. Daraei, H., Mittal, A., Mittal, J. & Kamali, H. Optimization of Cr(VI) removal onto biosorbent eggshell membrane: experimental and theoretical approaches. *Desalin. Water Treat.* **52**(7–9), 1307–1315 (2013).
59. Filardo, G., Di Matteo, B., Kon, E., Merli, G. & Marcacci, M. Platelet-rich plasma in tendon-related disorders: results and indications. *Knee Surg. Sports Traumatol. Arthrosc.* **26**(7), 1984–1999 (2018).
60. Eppley, B. L., Woodell, J. E. & Higgins, J. Platelet quantification and growth factor analysis from platelet-rich plasma: implications for wound healing. *Plast. Reconstr. Surg.* **114**(6), 1502–1508 (2004).
61. Marx, R. E. Platelet-rich plasma (PRP): what is PRP and what is not PRP? *Implant Dent.* **10**(4), 225–228 (2001).
62. Paoloni, J., De Vos, R. J., Hamilton, B., Murrell, G. A. & Orchard, J. Platelet-rich plasma treatment for ligament and tendon injuries. *Clin. J. Sport Med.* **21**(1), 37–45 (2011).
63. Andia, I., Sanchez, M. & Maffulli, N. Tendon healing and platelet-rich plasma therapies. *Expert Opin. Biol. Ther.* **10**(10), 1415–1426 (2010).
64. Mishra, A., Woodall, J. Jr. & Vieira, A. Treatment of tendon and muscle using platelet-rich plasma. *Clin. Sports Med.* **28**(1), 113–125 (2009).
65. Kajikawa, Y. et al. Platelet-rich plasma enhances the initial mobilization of circulation-derived cells for tendon healing. *J. Cell. Physiol.* **215**(3), 837–845 (2008).
66. Mahmoodabadi, R. A., Golafshan, H. A., Pezeshkian, F., Shahriarirad, R. & Namazi, M. Evaluation of the effect of platelet-rich fibrin matrix in the correction of periorbital wrinkles: an experimental clinical trial. *Dermatol. Pract. Concept.* **13**(1) (2023).
67. Elhambakhsh, A., Ghanaatian, A. & Keshavarz, P. Glutamine functionalized iron oxide nanoparticles for high-performance carbon dioxide absorption. *J. Nat. Gas Sci. Eng.* **94**, 104081 (2021).
68. Ghanaatian, A. et al. Coating SiO2 nanoparticles with polyvinyl alcohol for interfacial tension alteration in the system CO2 + polyethylen glycol + water. *Surf. Interfaces* **32**, 102164 (2022).
69. Rönicke, R. et al. Abeta mediated diminution of MTT reduction—an artefact of single cell culture? *PLoS One* **3**(9), e3236 (2008).
70. Hsiao, W. L., Mo, Z. Y., Fang, M., Shi, X. M. & Wang, F. Cytotoxicity of PM(2.5) and PM(2.5–10) ambient air pollutants assessed by the MTT and the Comet assays. *Mutat. Res.* **471**(1–2), 45–55 (2000).
71. Zare, M. R. et al. Antimicrobial core-shell electrospun nanofibers containing Ajwain essential oil for accelerating infected wound healing. *Int. J. Pharm.* **603**, 120698 (2021).
72. Locke, R. C., Ford, E. M., Silbernagel, K. G., Kloxin, A. M. & Killian, M. L. Success criteria for preclinical testing of cell-instructive hydrogels for tendon regeneration. *Tissue Eng. Part. C Methods* **26**:506–518
73. Meimandi-Parizi, A., Oryan, A. & Moshiri, A. Tendon tissue engineering and its role on healing of the experimentally induced large tendon defect model in rabbits: a comprehensive in vivo study. *PLoS One* **8**(9), e73016 (2013).
74. Yang, Z. et al. Effect of tendon stem cells in chitosan/β-glycerophosphate/collagen hydrogel on Achilles tendon healing in a rat model. *Med. Sci. Monit.* **24**, 4633 (2018).
75. Backman, C., Boquist, L., Fridén, J., Lorentzon, R. & Toolanen, G. Chronic achilles paratenonitis with tendinosis: an experimental model in the rabbit. *J. Orthop. Res.* **8**(4), 541–547 (1990).
76. Livak, K. J. & Schmittgen, T. D. Analysis of relative gene expression data using real-time quantitative PCR and the 2−ΔΔCT method. *Methods* **25**(4), 402–408 (2001).
77. Webb, W. R. et al. The application of poly(3-hydroxybutyrate-co-3-hydroxyhexanoate) scaffolds for tendon repair in the rat model. *Biomaterials* **34**(28), 6683–6694 (2013).
78. Sun, J. et al. Controlled release of collagen-binding SDF-1α from the collagen scaffold promoted tendon regeneration in a rat Achilles tendon defect model. *Biomaterials* **162**, 22–33 (2018).
79. Gabler, C. et al. In vivo evaluation of different collagen scaffolds in an Achilles tendon defect model. *Biomed Res. Int.* **2018** (2018).
80. Panheleux, M. et al. Organic matrix composition and ultrastructure of eggshell: a comparative study. *Br. Poult. Sci.* **40**(2), 240–252 (1999).
81. Richards, P. D., Botha, A. & Richards, P. A. Morphological and histochemical observations of the organic components of ostrich eggshell. *J. S Afr. Vet. Assoc.* **73**(1), 13–22 (2002).
82. Torres-Mansilla, A. et al. Eggshell membrane as a biomaterial for bone regeneration. *Polymers (Basel)* **15**(6), 1342 (2023).
83. Choi, J. et al. Eggshell membrane/gellan gum composite hydrogels with increased degradability, biocompatibility, and anti-swelling properties for effective regeneration of retinal pigment epithelium. *Polymers (Basel)* **12**(12), 2941 (2020).
84. Choi, H. J., Kim, Y. M., Suh, J. Y. & Han, J. Y. Beneficial effect on rapid skin wound healing through carboxylic acid-treated chicken eggshell membrane. *Mater. Sci. Eng. C Mater. Biol. Appl.* **128**, 112350 (2021).
85. Mensah, R. A. et al. The eggshell membrane: a potential biomaterial for corneal wound healing. *J. Biomater. Appl.* **36**(5), 912–929 (2021).
86. Gharibi, H. & Abdolmaleki, A. Thermo-chemical modification of a natural biomembrane to induce mucoadhesion, pH sensitivity and anisotropic mechanical properties. *J. Mech. Behav. Biomed. Mater.* **87**, 50–58 (2018).
87. Tavassoli, M. Effect of the substratum on the growth of CFU-c in continuous marrow culture. *Experientia* **39**(4), 411–412 (1983).
88. Vuong, T. T. et al. The extracellular matrix of eggshell displays anti-inflammatory activities through NF-kappaB in LPS-triggered human immune cells. *J. Inflamm. Res.* **10**, 83–96 (2017).
89. Circi, E. et al. Impact of platelet-rich plasma injection timing on healing of Achilles tendon injury in a rat model. *Acta Orthop. Traumatol. Turc.* **50**(3), 366–372 (2016).

90. Parafioriti, A. et al. Single injection of platelet-rich plasma in a rat Achilles tendon tear model. *Muscles Ligaments Tendons J.* **1**(2), 41–47 (2011).
91. Gautron, J. et al. Avian eggshell biomineralization: an update on its structure, mineralogy and protein tool kit. *BMC Mol. Cell. Biol.* **22**(1), 11 (2021).
92. Proudfoot, D. Calcium signaling and tissue calcification. *Cold Spring Harb Perspect. Biol.* **11**(10), a035303 (2019).
93. Molloy, T., Wang, Y. & Murrell, G. The roles of growth factors in tendon and ligament healing. *Sports Med.* **33**(5), 381–394 (2003).
94. Yu, Y. H. et al. Tri-layered doxycycline-, collagen- and bupivacaine-loaded poly(lactic-co-glycolic acid) nanofibrous scaffolds for tendon rupture repair. *Polymers (Basel)* **14**(13), 2659 (2022).
95. Gabler, C. et al. In vivo evaluation of different collagen scaffolds in an Achilles tendon defect model. *Biomed. Res. Int.* **2018**, 6432742 (2018).
96. Eliasson, P., Andersson, T. & Aspenberg, P. Influence of a single loading episode on gene expression in healing rat Achilles tendons. *J. Appl. Physiol.* **112**(2), 279–288 (2012).
97. Xu, Y. et al. Cyclic tensile strain induces tenogenic differentiation of tendon-derived stem cells in bioreactor culture. *Biomed. Res. Int.* **2015**, 790804 (2015).
98. Sugimoto, Y. et al. Scx+/Sox9+ progenitors contribute to the establishment of the junction between cartilage and tendon/ligament. *Development* **140**(11), 2280–2288 (2013).
99. Subramanian, A. & Schilling, T. F. Tendon development and musculoskeletal assembly: emerging roles for the extracellular matrix. *Development* **142**(24), 4191–4204 (2015).
100. Sinn, H. P. et al. Comparison of immunohistochemistry with PCR for assessment of ER, PR, and Ki-67 and prediction of pathological complete response in breast cancer. *BMC Cancer* **17**(1), 124 (2017).

Acknowledgements
None.

Author contributions
S.A.E, N.T., and O.K.H designed the study. O.K.H., R.S., A.D., L.A., S.B., A.D., O.A., S.P.K., S.H., A.A.M., R.K., collected the data and performed the laboratory evaluations. R.S. drafted the manuscript. S.A.E., N.T., and O.K.H revised the manuscript. All authors read and confirmed the final version of the manuscript.

Declarations

Competing interests
The authors declare no competing interests.

Ethics approval and consent to participate
All experimental protocols were approved by the Institutional Animal Care and the Ethics Committee of the Shiraz University of Medical Science. Also, the study was carried out in compliance in accordance with the relevant guidelines and regulations and the Declaration of Helsinki and also the ARRIVE guidelines.

Additional information
Correspondence and requests for materials should be addressed to R.S. or N.T.

Reprints and permissions information is available at www.nature.com/reprints.

Publisher's note Springer Nature remains neutral with regard to jurisdictional claims in published maps and institutional affiliations.